Stiffness anisotropy of a natural clay at small strains

L'anisotropie de la rigidité d'une argile à petites déformationes

S.Rampello – *University of Messina, Italy*
L.Callisto – *University of Rome 'La Sapienza', Italy*

ABSTRACT: In this paper, the small-strain stiffness of a natural clay has been studied using a triaxial cell instrumented with local displacement transducers and with three pairs of bender elements, to measure the shear wave velocities in the vertical and the horizontal planes. Bender element tests were carried out at different values of mean effective stress, on samples compressed along constant stress ratio paths. Such measurements permitted to evaluate the dependence of small-strain shear stiffness on current stress state and past stress history and the stiffness anisotropy at small strains. The shear modulus obtained at small strains from undrained stress-strain relationships was seen to be in a fair agreement with that obtained from bender element measurements.

RÉSUMÉ: Dans ce papier, on étudie la rigidité à petites déformationes d'une argile naturelle, au moyen d'un appareil de compression triaxiale, équipé de trois couples de languettes piezoelectriques vibrantes et des jauges axiales locales. On a donc pu mesuré la vélocité des ondes de cisaillement dans les planes vertical et horizontal, à plusieurs valeurs de la contrainte moyenne intergranulaire, en compriment le sol le long des parcours avec des rapports constant de contrainte. Ces essais ont permis de déterminer la variation de la rigidité à petites déformationes en fonction de la contrainte moyenne courante, et l'anisotropie de la rigidité à petites déformationes. Les valeurs de la rigidité à petites déformationes obtenues par les courbes contrainte-déformation et celles mesurées avec les languettes piezoelectriques sont assez similaires.

1 INTRODUCTION

Small-strain deformation characteristics of stiff clays are of the utmost importance in geotechnical engineering when dealing with static or dynamic deformation problems. Modelling pre-failure soil behaviour at small strains is usually done following the empirical approach of the variable moduli formulations, or adopting plasticity-based soil models. In the latter case, the non linear behaviour observed at small-strains is often interpreted as resulting from development of plastic strains within a bounding surface. Models proposed in the framework of hardening plasticity include a kinematic yield surface inside the boundary surface, which define the extension of the elastic domain (e.g.: Stallebrass & Taylor, 1997; Rouania & Muir Wood, 2000; Kavvadas & Amorosi, 2000). When using such models, it is necessary to define the size of the inner yield locus and to choose the particular form of elasticity to be used within the surface. To date, the assumption of isotropic poro-elasticity is usually made inside this locus.

On the other hand, increase of local instrumentation installed on the samples has recently permitted accurate evaluation of stiffness anisotropy starting from very small strains.

The small-strain shear stiffness of soils can be measured in the laboratory by dynamic testing techniques using the piezoceramic bender element transducers. Use of multi-directional bender element trasducers has recently permitted to study the anisotropy of shear stiffness at small strains (Jovicic & Coop, 1998; Kuwano et al., 1999; Nash et al., 1999). In these studies, the degree of anisotropy was expressed by the ratio of the shear modulus on the horizontal plane $G_{0(hh)}$ to the one in the vertical planes $G_{0(vh)}$.

In this paper, the small-strain shear stiffness of natural samples of a stiff clay was measured in the triaxial apparatus during isotropic and anisotropic compression. To this purpose, three pairs of differently oriented bender elements were used. Test results confirmed that the clay is anisotropic with respect to stiffness and also demonstrated that the small-strain stiffness increases with increasing effective stress ratio experienced by the samples during constant-η compression paths.

2 TESTING PROGRAMME

Triaxial tests were carried out on 38 mm diameter, 76 mm high specimens in a stress-path controlled triaxial cell. Local instrumentation consisted of one pair of axial strain inclinometers (Ackerley et al. 1987) and three couples of bender elements (Dyvik & Madshus 1985). The vertical bender elements were installed into the top and bottom platens of the cell, while the lateral elements were mounted at sample mid-height in probes which were inserted through the membrane in rubber grommets (Nash et al. 1999).

Lateral benders measured the velocities V_{hv} and V_{hh} of vertically and horizontally polarised shear waves propagating in the horizontal direction, while vertical benders measured the velocity V_{vh} of horizontally polarised shear waves propagating vertically (Fig. 1).

The length of the wave travel path was taken as the distance between the tips of the benders (Viggiani & Atkinson 1995). A square input wave with a frequency of 50 Hz and an amplitude of ±10 V was used to drive the transmitter element. The arrival time of the shear wave was selected as the average of time distances Δt_1 and Δt_2 shown in Fig. 2 (Viggiani & Atkinson 1995).

The testing programme was carried out on natural samples of Pietrafitta Clay, of lacustrine origin. Large block samples were taken from an open cast mine; samples were retrieved from a depth of about 2 m below the current ground surface, underneath the unexploited lowermost portion of the lignite layer. Mechanical properties of Pietrafitta Clay have been studied by Rampello (1994), Rampello & Silvestri (1993), Burland et al. (1996). Table 1 reports the average physical and index properties of the material tested. The soil is a high plasticity clay with a clay fraction in excess of 80 % and a negligible content of calcium carbonate.

Bender element measurements were made at points along radial effective stress paths with constant values of $\eta = q/p'$ equal to 0 and 0.5, starting from the residual mean effective stress $p'_k = 250$ kPa measured in the samples (Fig. 3). Undrained compression tests were carried out on the samples after unloading to 400 kPa and 250 kPa, respectively.

Table 1. Physical and index properties of Pietrafitta Clay

γ (kN/m^3)	G_s	W_0 (%)	e_0	W_L (%)	I_P (%)	CF (%)
17.3	2.6	45.3	1.178	95.5	60.9	84

3 EXPERIMENTAL RESULTS

In the following, the shear stiffness of Pietrafitta Clay is conventionally discussed in terms of cross-anisotropic elasticity, although soil behaviour is known to be inelastic even at small strain levels. Elastic shear moduli should then be regarded simply as a tool to interpret test results.

The bender element tests were interpreted assuming that the soil behaves as an ideal linear elastic continuum and that the waves propagate in an infinite space; also, the effects of boundary conditions associated with sample and apparatus geometry were neglected. In these hypotheses the small-strain shear modulus is evaluated as

$$G_{0(ij)} = \rho \cdot V_{ij}^2 \tag{1}$$

where ρ is the current mass density and the indexes i and j are the propagation and polarisation directions of the shear waves, respectively.

For test *TX*-0.5, the small-strain shear moduli $G_{0(ij)}$, divided by the reference pressure p_r = 1 kPa, are plotted against the ratio p'/p_r on a bilogarithmic scale (Fig. 4(a)) while the non dimensional shear moduli $G_{0(ij)}/p_r$ are plotted against the specific volume v on a semilogarithmic scale (Fig. 4(b)). The dependence of $G_{0(ij)}$ on p' and v shown in Fig. 4 is also representative of the behaviour observed for the isotropically compressed sample: $G_{0(ij)}$ increases with increasing mean effective stress and decreasing specific volume. The G_0/p_r - p'/p_r relationships show a slight upward concavity as the stress paths approach the mean effective yield stress p'_y = 700 kPa, measured in isotropic compression tests. At the same mean effective stress, the small-strain shear modulus in the horizontal planes $G_{0(hh)}$ is larger than the shear moduli $G_{0(vh)}$ and $G_{0(hv)}$, evaluated in the vertical planes.

The ratio of the small-strain shear moduli in the horizontal and vertical planes $G_{0(hh)}/G_{0(hv)}$, plotted against p' in Fig. 5, is not affected by the mean effective stress and is in the range 1.15 to 1.3. Hence, for both the investigated stress ratios natural Pietrafitta Clay exhibits values of the small-strain shear modulus $G_{0(hh)}$ about 22.5 % higher than that of $G_{0(hv)}$.

For anisotropic stress states, the dependence of the small-strain shear modulus on the current state can be expressed in the form (Rampello et al., 1997):

$$\frac{G_{0(ij)}}{p_r} = S_{\eta(ij)} \cdot \left(\frac{p'}{p_r}\right)^n \left(\frac{p'_{e\eta}}{p'}\right)^c \tag{2}$$

where p_r = 1 kPa is a reference stress, $S_{\eta(ij)}$, n and c are material constants and

$$p'_{e\eta} = p_r \cdot \exp\left(\frac{N_\eta - v}{\lambda}\right) \tag{3}$$

is the equivalent mean effective stress measured on the constant-η normal compression line (η-NCL). In equation (3), N_η is the specific volume on the η-NCL at $p' = p_r$, v is the current specific volume, λ is the slope of the η-NCL in the v-ln p' plane. In equation (2), p' accounts for the dependence of G_0 on the current stress state, while $p'_{e\eta}$ accounts for the effects of specific volume and past stress history.

In this work, bender element tests were carried out on samples compressed along radial effective stress paths with constant values of η equal to 0 and 0.5. The influence of different compression histories was evaluated taking the samples compressed isotropically as a reference for comparison.

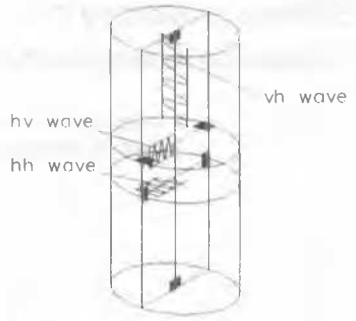

Fig. 1. Arrangement of bender elements in the triaxial sample.

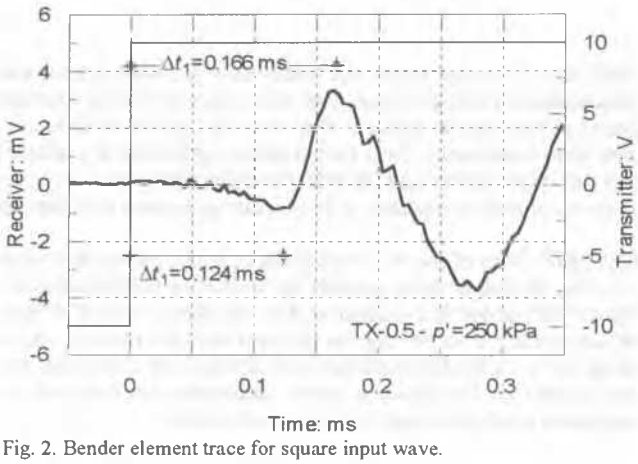

Fig. 2. Bender element trace for square input wave.

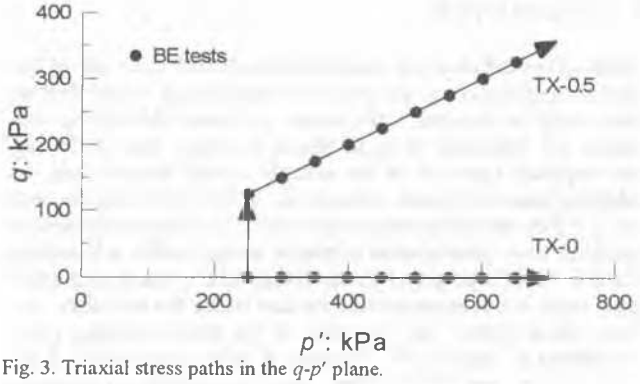

Fig. 3. Triaxial stress paths in the q-p' plane.

Therefore, the experimental results were normalised by the equivalent pressure determined on the isotropic normal compression line characterised by N = 3.75 and λ = 0.25.

Dividing both sides of eqn. (2) by the equivalent pressure on the isotropic compression line p'_e raised to the power $(n\text{-}c)$, the following expression is obtained:

$$\left(\frac{G_{0(ij)}}{p_r}\right)\left(\frac{p_r}{p'_e}\right)^n = S_{e(ij)} \cdot \left(\frac{p'}{p'_e}\right)^{(n-c)} \tag{4}$$

with

$$S_{e(ij)} = S_{\eta(ij)} \cdot \left(\frac{p'_{e\eta}}{p'_e}\right)^c = S_{\eta(ij)} \cdot \exp\left[\frac{c}{\lambda}(N_\eta - N)\right] \tag{5}$$

where $(N_\eta\text{-}N)$ is the vertical distance between the isotropic and constant-η normal compression lines in a v-ln p' plane.

In Fig. 6(a)-(b), the quantities $[(G_{0(ij)}/p_r)(p_r/p'_e)^n]$ are plotted against the ratio p'/p'_e on a bilogarithmic scale. After normalisation, data points plot closely around parallel best fit lines obtained using a slope $(n\text{-}c)$ = 0.32, irrespective of the value of η during compression; this figure was derived averaging the slopes of the best-fit lines of each set of data.

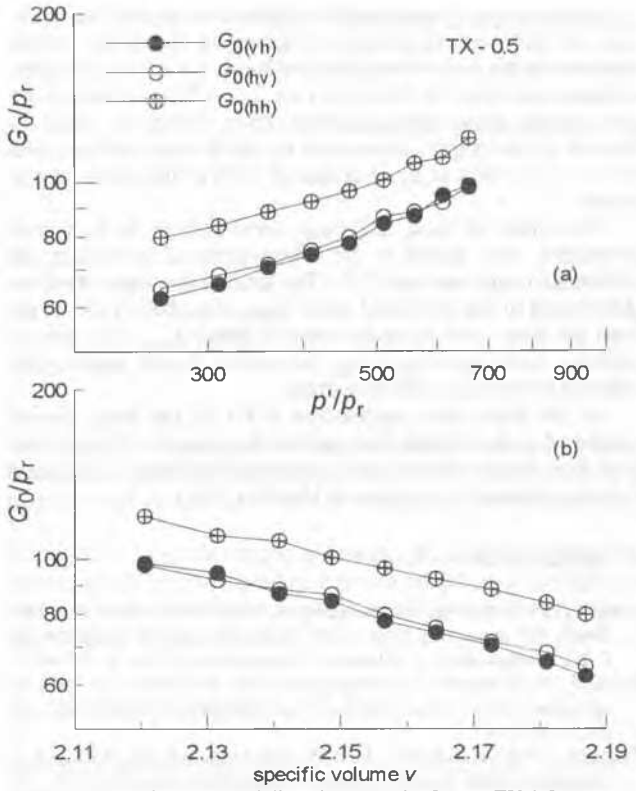

Fig. 4. Small-strain shear moduli against p' and v for test TX-0.5.

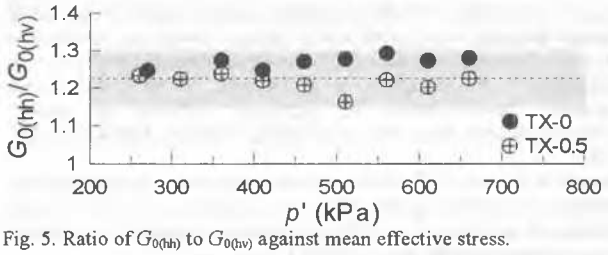

Fig. 5. Ratio of $G_{0(hh)}$ to $G_{0(hv)}$ against mean effective stress.

Parallelism between the lines permitted to quantify differences in shear stiffness using the ratio of the stiffness multipliers $S_{e(ij)}$, which define the position of the regression lines in the normalised plane. For each value of η, different lines interpolate data relative to the values of $G_{0(hh)}$, $G_{0(hv)}$ and $G_{0(vh)}$; the corresponding values of the stiffness coefficients $S_{e(hh)}$, $S_{e(hv)}$ and $S_{e(vh)}$ are reported in Table 2 together with the average coefficient $S_{e(v)} = (S_{e(hv)} + S_{e(vh)})/2$ used to quantify the shear stiffness in the vertical plane. The ratio of $S_{e(hh)}$ to $S_{e(v)}$ measures the stiffness anisotropy and is about 1.23.

Table 2. Values of S_e obtained from bender element tests.

Test	η	$S_{e(hh)}$	$S_{e(hv)}$	$S_{e(vh)}$	$S_{e(v)}$	$S_{e(hh)}/S_{e(v)}$
TX-0	0	597	470	492	481	1.24
TX-0.5	0.5	651	536	528	532	1.22

When normalising data with respect to the isotropic equivalent mean effective stress, the implicit assumption is made that the small-strain shear stiffness depends solely on mean effective stress and void ratio. The differences still observed after normalisation can then be attributed to the influence of different strain histories which are likely to produce different particle arrangements at the same void ratio. Therefore, the effect of η can be evaluated by the ratios of $S_{e(hh)}$ and $S_{e(v)}$ to the corresponding values observed for isotropic stress history (η = 0). For η = 0.5 these ratios are about 1.1, indicating that the deviator stress applied in this case produces, for the same values of p', an increase of about 10 % in soil stiffness.

Figure 7(a)-(b) shows undrained stress-strain relationships for the samples sheared after isotropic and anisotropic compression.

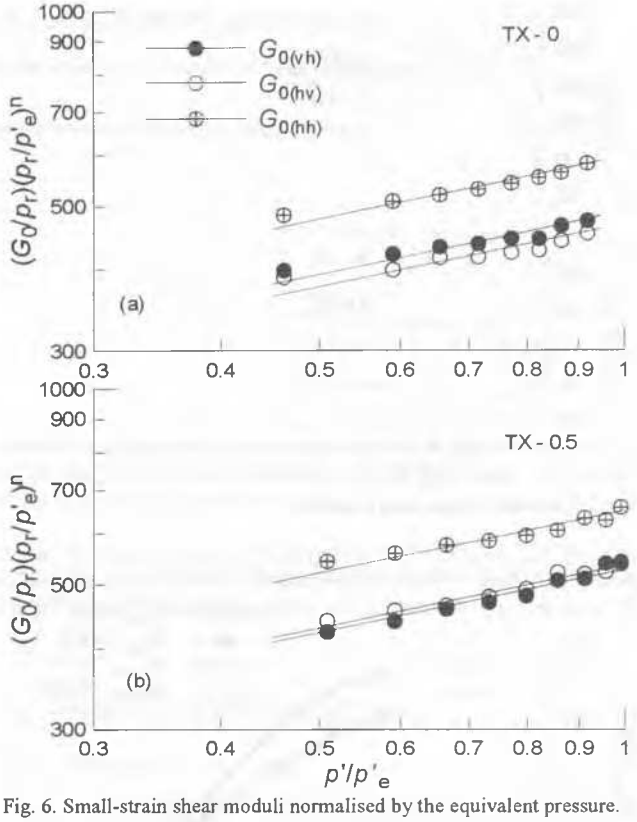

Fig. 6. Small-strain shear moduli normalised by the equivalent pressure.

Undrained shearing was carried out after swelling from a maximum previous mean effective stress p' = 660 kPa; sample TX – 0 was isotropically swelled to p' = 400 kPa, while sample TX – 0.5 was swelled under a constant stress ratio η = 0.5 to p' = 250 kPa. The samples showed brittle behaviour with the formation of rupture planes resulting in reductions in strength. Shear strain at peak strength was about 2.5 % for shearing after isotropic stress history, while it was as low as about 1% after constant-η loading-unloading paths.

In Fig. 8 the equivalent secant shear modulus $G_{eq} = \Delta q/3\Delta\varepsilon_s$, obtained from the stress-strain curves using the local measurements of axial displacement, is plotted against the shear strain $\varepsilon_s = 2(\varepsilon_a - \varepsilon_r)/3$ where the subscripts a and r refer to axial and radial directions, respectively. Axial strains were resolved down to 0.002 %. The higher stiffness observed for the isotropically compressed samples should be ascribed to the higher initial mean effective stress.

In order to compare static and dynamic measurements of shear stiffness at small strains, values of $G_{0(hh)}$ and $G_{0(hv)}$ must be converted into an equivalent isotropic shear modulus $G_{0(eq)}$. To this purpose the form of anisotropy proposed by Graham & Houlsby (1983) was used. The anisotropy parameter α can be defined as:

$$\alpha = G_{0(hh)}/G_{0(hv)} \cdot \qquad (6)$$

Assuming ν_{vh} = 0.1 the vertical and horizontal Young's moduli E'_v and E'_h can be calculated as

$$E'_v = 2\left(G_{0(vh)}/\alpha\right)\cdot\left(1+\nu_{vh}\cdot\alpha\right); \quad E'_h = \alpha^2 \cdot E'_v \qquad (7)$$

From the direction of the undrained stress path derived by Graham & Houlsby (1983)

$$\frac{dq}{dp'} = 3\cdot\left[\frac{(1-\alpha\nu_{vh})-2\alpha^2\nu_{vh}+\alpha^2/2}{(1-\alpha\nu_{vh})+\alpha^2\nu_{vh}-\alpha^2}\right] \qquad (8)$$

the incremental stress ratio is obtained

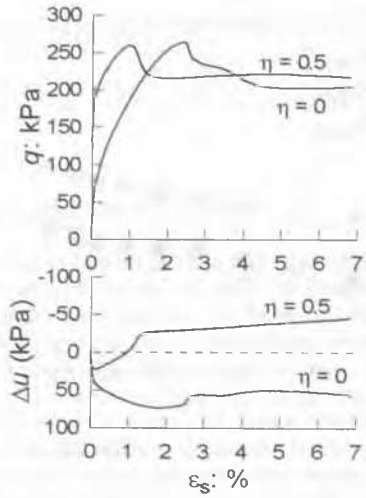

Fig. 7. Undrained stress-strain behaviour

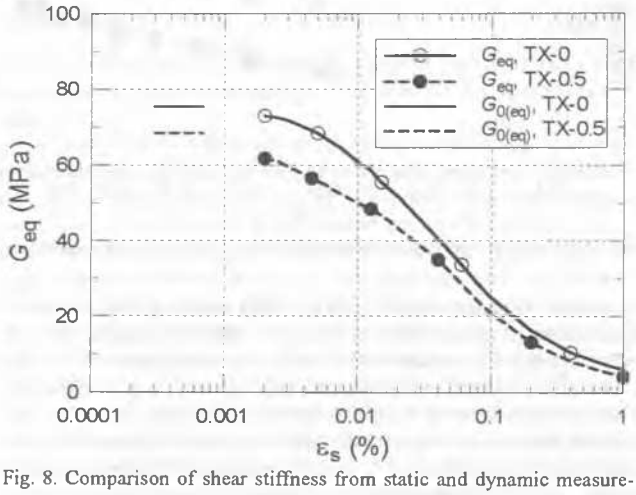

Fig. 8. Comparison of shear stiffness from static and dynamic measurements.

$$\frac{d\sigma'_a}{d\sigma'_r} = \frac{3+2dq/dp'}{3-dq/dp'} \quad (9)$$

and the axial and radial strains can be evaluated by the usual constitutive equations for cross-anisotropic elasticity. The equivalent isotropic shear modulus is finally obtained as $G_{0(eq)} = \Delta q/3\Delta\varepsilon_s$.

Values of $G_{0(eq)}$ evaluated from bender element tests are plotted in Fig. 8 for shear strains smaller than 0.001 %. A fair agreement is observed at small-strains between static and dynamic measurements of the equivalent isotropic shear modulus, the dynamic measurements yielding values of $G_{0(eq)}$ from 3 % to 10 % higher than the static ones measured at ε_s = 0.002 %.

These results confirm that a satisfactory agreement is generally obtained between static and dynamic measurements of small-strain shear stiffness, provided that local transducers are used for measuring sample deformations in static tests (e.g.: Georgiannou et al., 1991; Rampello & Silvestri, 1993; Connolly & Kuwano, 1999).

4 CONCLUSIONS

Stress-path controlled tests were carried out on natural samples of a stiff clay using a triaxial cell instrumented with multi-directional bender elements. Small-strain stiffness was studied on samples compressed under radial stress paths with constant values of the stress ratio η. Three pairs of bender elements were used to determine the shear moduli $G_{0(vh)}$, $G_{0(hv)}$ and $G_{0(hh)}$.

Interpretation of tests results permitted to quantify the influence of different compression histories on the shear moduli measured at the same mean effective stress. For η = 0.5 the shear stiffness was about 10 % higher than the stiffness measured under isotropic stress conditions; this shows a relatively small influence of anisotropic compression on small-strain stiffness even for η = 0.5, which is equal to almost 70 % of the stress ratio at failure.

The values of $G_{0(vh)}$ and $G_{0(hv)}$ were seen to be in a good agreement, as it should be for a homogeneous continuum, the difference being less than 5 %. The small-strain shear modulus determined in the horizontal plane $G_{0(hh)}$ was about 22 % larger than the shear modulus in the vertical plane $G_{0(hv)}$. The ratio of stiffness anisotropy $G_{0(hh)}/G_{0(hv)}$ was seen to be not significantly affected by the mean effective stress.

As the shear strain approaches 0.001 %, the shear moduli measured in the triaxial tests tend to the values of $G_{0(eq)}$ evaluated from bender element tests, assuming the form of transverse isotropy proposed by Graham & Houlby (1983).

5 REFERENCES

Ackerley, S.K., Hellings, J.E. & Jardine, R.J. 1987. Discussion on A new device for measuring local axial strains on triaxial specimens by C.R.I. Clayton and S.A. Khatrush, *Géotechnique* **37**, No. 3, 413-417.

Burland, J.B., Rampello, S., Georgiannou, V.N. & Calabresi, G. 1996. A laboratory study of the strength of four stiff clays. *Géotechnique*, **46**, No. 3, 491-514.

Connolly, T.M. & Kuwano, R. 1999. The measurement of G_{max} in a resonant column, bender element, torsional shear apparatus. *Proc. 2nd Int. Symp. on Pre-Failure Deformation Characteristics of Geomaterials – IS Torino 99*. Torino, Balkema, **1**, 73-80.

Dyvik, R. & Madshus, C. 1985. Laboratory measurements of G_{max} using bender elements. *Proc. of the ASCE Annual Convention: advances in the art of testing soils under cyclic conditions*. Detroit:186-196.

Georgiannou, V.N., Rampello, S. & Silvestri, F. 1991. Static and dynamic measurements of undrained stiffness of natural overconsolidated clays. *Proc. X ECSMFE*, Florence, Balkema, **1**, 91-95.

Graham J. & Houlsby G.T. 1983. Anisotropic elasticity of a natural clay. *Géotechnique* **33**, No.2, 165-180.

Kavvadas, M. & Amorosi, A. 2000. A consitutive model for structured soils. *Géotecnique* **50**, No. 3, 263-273.

Kuwano, R., Connolly, T.M. & Kuwano, J. 1999. Shear stiffness anisotropy measured by multi-directional bender element transducers. *Proc. 2nd Int. Symp. on Pre-Failure Deformation Characteristics of Geomaterials – IS Torino 99*. Torino, Balkema, **1**, 205-212.

Jovicic, V. & Coop, M.R. 1998. The measurement of stiffness anisotropy in clays with bender element tests in the triaxial apparatus. *Geotechnical Testing Journal* **21**, No. 1, 3-10.

Nash, D.F.T., Pennington, D.S. & Lings, M.L. 1999. The dependence of anisotropic G_0 shear moduli on void ratio and stress state for reconstituted Gault clay. *Proc. 2nd Int. Symp. on Pre-Failure Deformation Characteristics of Geomaterials – IS Torino 99*. Torino, Balkema, **1**, 229-238.

Rampello, S. 1994. Observed behaviour of large diameter bored piles in medium to stiff clay. *Int. Workshop on "Pile Foundations: Experimental Investigations, Analysis and Design"*, Università degli Studi di Napoli Federico II, Napoli, 261-301.

Rampello, S. & Silvestri, F. 1993 The stress-strain behaviour of natural and reconstituted samples of two overconsolidated clays. *Proc. 1st Int. Symp. on Geotechnical Engineering of Hard Soils – Soft Rocks*. Athens, Balkema, **1**, 769-778.

Rampello S., Viggiani, G.M.B. & Amorosi, A. 1997. Small-strain stiffness of reconstituted clay compressed along constant triaxial effective stress ratio paths. *Géotechnique* **47**, No. 3, 475-489.

Rouania, M. & Muir Wood, D. 2000. A kinematic hardening constitutive model for natural clays with loss of structure. *Géotechnique* **50**, No. 2, 153-164.

Stallebrass S.E. & Taylor R.N. 1997. The development and evaluation of a constitutive model for the prediction of ground movements in overconsolidated clays. *Géotechnique* **47**, No. 2, 235-253.

Viggiani, G. & Atkinson, J.H. 1995. The interpretation of the bender element tests. Technical Note, *Géotechnique*, **45**, No. 1, 149-154.